

Isotropic-nematic transition of hard rods immersed in random sphere matrices

Matthias Schmidt^{a)} and Marjolein Dijkstra

Debye Institute, Soft Condensed Matter Group, Utrecht University, Princetonplein 5, 3584 CC Utrecht, The Netherlands

(Received 4 June 2004; accepted 21 September 2004)

Using replica density functional theory and Monte Carlo computer simulations we investigate a system of annealed hard spherocylinders adsorbed in a matrix of quenched hard spheres. Theoretical predictions for the partition coefficient, defined as the ratio of density of rods in the matrix and that in a reservoir, agree well with simulation results. Theory predicts the isotropic-nematic transition to remain first order upon increasing sphere packing fraction, and to shift towards lower rod densities. This scenario is consistent with our simulation results that clearly show a jump in the nematic order parameter upon increasing the rod density at constant matrix packing fraction, corresponding to the isotropic-nematic transition, even for sphere matrix packing fractions $\lesssim 0.3$. © 2004 American Institute of Physics. [DOI: 10.1063/1.1815294]

I. INTRODUCTION

The effect of quenched disorder on the isotropic-nematic phase transition is a matter of strong current interest and a variety of experimental, simulation, and theoretical techniques have been used to reveal the nature of orientational order. The Imry-Ma argument¹ prohibits the existence of true long-range order in a nematic phase exposed to quenched random orienting fields. The question what happens instead when long-range order is disrupted in nematics with quenched disorder has been addressed recently,² and also dynamical aspects have been considered.³ Quasi-long-range order, however, exists in nematics confined in random porous media.⁴ Simulation evidence was given for critical behavior of the isotropic-nematic phase transition in a porous medium.⁵ Much work has been devoted to phenomenological approaches, to rotator lattice models, and the Maier-Saupe model (see Ref. 6 for recent work on the orientational relaxation of this model). A related binary system is that of colloidal particles dispersed in a liquid crystal, see, e.g., Ref. 7 for recent work on capillary condensation of the nematic phase between two spherical particles dispersed in a bulk isotropic phase.

Nematic ordering in bulk can be understood on a microscopic level via excluded volume interactions of particles with continuous spatial and orientational degrees of freedom. The Onsager isotropic-nematic transition of the hard rod fluid is a prominent example of a phase transition in such a system.⁸ To study orientationally ordered phases density-functional theory⁹ is a primary tool, and in fact Onsager's theory is based on the low-density expansion of the (exact) free energy functional. For additive hard sphere mixtures Rosenfeld's (nonperturbative) fundamental-measure theory (FMT) (Ref. 10) provides a very accurate description. Early

extensions thereof to arbitrary convex bodies were given^{11,12} and modified to describe the isotropic-nematic transition of hard spherocylinders and ellipsoids.¹³ Recently, a technical difficulty was overcome and the so-called deconvolution of the Mayer bond into functions characteristic for single particles was obtained for mixtures of spheres and (thin) rods;^{14–16} other cases have also been considered.¹⁷ The rod-sphere functional predicts the properties of the free interface between demixed fluid phases very reliably as compared to simulations,¹⁸ and has also been used to study the wetting behavior at a planar hard wall.¹⁹

One approach to model porous substances is to rely on immobilized particle configurations of model fluids. These configurations are “quenched,” and are brought into contact with an equilibrated “annealed” fluid. The conventional tool to study such quenched-annealed (QA) mixtures is via the replica trick, and a variety of liquid state integral equations have been carried over from equilibrium to QA models. Recently, a density functional theory (DFT) approach to such QA models was proposed^{20,21} and demonstrated to give good account of hard sphere correlations,²⁰ capillary condensation and evaporation,^{22,23} surface behavior of hard spheres,²⁴ freezing in a lattice model,²⁵ and the structure of hard spheres immersed in random fiber networks.²⁶

In this work we combine the tools developed in Refs. 14, 15, 20, and 21 to arrive at a replica DFT for annealed hard rods in the Onsager limit of large length-to-thickness size ratios immersed in a matrix of quenched spheres. We consider two types of interactions between matrix particles, namely, hard sphere and ideal (vanishing) interactions, the latter leading to more open matrix void structures at equal density. We find that the isotropic-nematic transition remains stable upon increasing density of matrix particles. The coexisting densities of rods in the void space, however, increase exponentially with increasing matrix densities. We compare these findings with results from computer simulations where we find a similar shift in the coexisting densities via analyz-

^{a)}On leave from Institut für Theoretische Physik II, Heinrich-Heine-Universität Düsseldorf, Universitätsstraße 1, D-40225 Düsseldorf, Germany.

ing the behavior of the nematic order parameter. Both approaches cannot access the true long-range behavior of the model. In simulations finite-size effects are present, and the DFT is essentially a mean-field treatment. We believe, however, that our findings describe what would be seen in a finite sample of colloidal rods immersed in a mesoporous material.²⁷

The paper is organized as follows. In Sec. II we define the model of thin hard rods immersed in a sphere matrix in more detail. We outline our DFT approach in Sec. III. The simulation techniques are briefly discussed in Sec. IV. Results from DFT and simulations are presented in Sec. V. We finish with concluding remarks in Sec. VI.

II. THE MODEL

We consider a fluid of needlelike hard rods (species N) of diameter D and length L , where $L \gg D$. The rods are immersed in a quenched matrix comprised of spheres of radius R (and diameter $\sigma = 2R$), and we restrict ourselves to the case of large spheres, $LD \ll \sigma^2$. The interaction between a fluid rod and a matrix sphere is that of hard bodies, i.e., infinite if both particles overlap and zero otherwise. We consider two different kinds of sphere-sphere interactions: (i) a hard sphere interaction, being infinite if the separation distance between spheres centers is $< 2R$ and zero otherwise and (ii) freely overlapping spheres that behave like an ideal gas (i.e., the pair interaction vanishes for all distances).

We denote the number densities of both species by ρ_i , $i = S, N$, and also use the sphere packing fraction $\eta = \pi \rho_S \sigma^3 / 6$ as a parameter. The size ratio L/σ is a geometric control parameter. Local density profiles for spheres and rods are denoted by $\rho_S(\mathbf{r})$ and $\rho_N(\mathbf{r}, \mathbf{\Omega})$, respectively, where \mathbf{r} is the space coordinate and $\mathbf{\Omega}$ is the rod orientation. See Fig. 1 for an illustration of the model.

III. DENSITY FUNCTIONAL THEORY

A. General strategy

Following the extension of DFT (Ref. 9) to QA mixtures^{20,21} we express the grand potential functional as

$$\Omega[\rho_S; \rho_N] = F_{\text{id}}[\rho_N] + F_{\text{exc}}[\rho_S; \rho_N] + \int d^3r \times \int \frac{d^2\Omega}{4\pi} \rho_N(\mathbf{r}, \mathbf{\Omega}) [V_{\text{ext}}(\mathbf{r}, \mathbf{\Omega}) - \mu_N], \quad (1)$$

where $V_{\text{ext}}(\mathbf{r}, \mathbf{\Omega})$ is an external potential acting on the rods (which will be set to zero in the following) and μ_N is the rod chemical potential. The ideal free energy functional is given by

$$F_{\text{id}}[\rho_N] = k_B T \int d^3r \int \frac{d^2\Omega}{4\pi} \rho_N(\mathbf{r}, \mathbf{\Omega}) \times [\ln(\rho_N(\mathbf{r}, \mathbf{\Omega}) \Lambda_N^3) - 1], \quad (2)$$

where Λ_N is the (irrelevant) thermal wavelength of the rods, k_B is the Boltzmann constant, and T is the absolute temperature. The effects of all interparticle interactions, those between rods and rods as well as those between rods and (quenched) spheres are described through the excess free en-

ergy functional F_{exc} . The following section is devoted to an explicit approximation thereof. The minimization condition is

$$\left. \frac{\delta \Omega[\rho_S; \rho_N]}{\delta \rho_N(\mathbf{r}, \mathbf{\Omega})} \right|_{\rho_S(\mathbf{r}')} = 0, \quad (4)$$

where the density distribution of the quenched species $\rho_S(\mathbf{r}')$ is treated as a fixed quantity.^{20,21} In the case of the freely overlapping matrix this is just the distribution of an ideal gas, for the hard sphere matrix it can be calculated from Rosenfeld's hard sphere functional.¹⁰

B. Excess free energy functional

Following the general structure of FMT (Ref. 10) and, in particular, the extension to QA fluids,²⁰ the (Helmholtz) excess free energy is obtained by integrating over a free energy density

$$F_{\text{exc}}[\rho_S; \rho_N] = k_B T \int d^3r \int \frac{d^2\Omega}{4\pi} \Phi(\{n_\nu^i\}), \quad (5)$$

where the (reduced) free energy density Φ is a simple function (not a functional) of the weighted densities n_ν^i , where $i = S, N$ labels the species and ν labels the type of weighted density. The functional form of Φ is obtained by consideration of the exact zero-dimensional excess free energy.²⁰ For the case of the hard sphere matrix $\Phi = \Phi_{\text{HSM}}$, where

$$\Phi_{\text{HSM}} = -n_0^N \ln(1 - n_3^S) + \frac{n_1^N n_2^{SN} + n_1^N n_2^{NN}}{1 - n_3^S}. \quad (6)$$

For ideal matrix spheres we find $\Phi = \Phi_{\text{IDM}}$, where

$$\Phi_{\text{IDM}} = n_0^N n_3^S + n_1^N n_2^{SN} + n_1^N n_2^{NN} \exp(n_3^S). \quad (7)$$

The dependence on the spatial coordinate \mathbf{r} and the orientation $\mathbf{\Omega}$ are suppressed in the notation in Eqs. (6) and (7); we give the explicit dependences and the relation to the bare density fields in the following. The weighted densities for rods are given by

$$n_0^N(\mathbf{r}, \mathbf{\Omega}) = \rho_N(\mathbf{r}, \mathbf{\Omega}) * w_0^N(\mathbf{r}, \mathbf{\Omega}), \quad (8)$$

$$n_1^N(\mathbf{r}, \mathbf{\Omega}) = \rho_N(\mathbf{r}, \mathbf{\Omega}) * w_1^N(\mathbf{r}, \mathbf{\Omega}), \quad (9)$$

$$n_2^{NN}(\mathbf{r}, \mathbf{\Omega}') = \int \frac{d^2\Omega}{4\pi} \rho_N(\mathbf{r}, \mathbf{\Omega}) * w_2^{NN}(\mathbf{r}, \mathbf{\Omega}; \mathbf{\Omega}'), \quad (10)$$

where the asterisk denotes the spatial convolution, $g(\mathbf{r}) * h(\mathbf{r}) = \int d^3x g(\mathbf{x}) h(\mathbf{r} - \mathbf{x})$, and the weight functions are defined as

$$w_0^N(\mathbf{r}, \mathbf{\Omega}) = \frac{1}{2} [\delta(\mathbf{r} + \mathbf{\Omega}L/2) + \delta(\mathbf{r} - \mathbf{\Omega}L/2)], \quad (11)$$

$$w_1^N(\mathbf{r}, \mathbf{\Omega}) = \frac{1}{4} \int_{-L/2}^{L/2} dl \delta(\mathbf{r} + \mathbf{\Omega}l), \quad (12)$$

$$w_2^{NN}(\mathbf{r}, \mathbf{\Omega}; \mathbf{\Omega}') = 16D \sqrt{1 - (\mathbf{\Omega} \cdot \mathbf{\Omega}')^2} w_1^N(\mathbf{r}, \mathbf{\Omega}), \quad (13)$$

where $\delta(\cdot)$ is the Dirac distribution. For spheres the weighted densities are

$$n_0^S(\mathbf{r}) = \rho_S(\mathbf{r}) * w_0^S(\mathbf{r}), \quad (14)$$

$$n_2^{SN}(\mathbf{r}, \mathbf{\Omega}) = \rho_S(\mathbf{r}) * w_2^{SN}(\mathbf{r}, \mathbf{\Omega}), \quad (15)$$

$$n_3^S(\mathbf{r}) = \rho_S(\mathbf{r}) * w_3^S(\mathbf{r}), \quad (16)$$

where the weight functions are given by

$$w_0^S(\mathbf{r}) = \delta(R-r)/(4\pi R^2), \quad (17)$$

$$w_2^{SN}(\mathbf{r}, \mathbf{\Omega}) = 2\delta(R-r) \left| \frac{\mathbf{r}}{r} \cdot \mathbf{\Omega} \right|, \quad (18)$$

$$w_3^S(\mathbf{r}) = \Theta(R-r), \quad (19)$$

with $r=|\mathbf{r}|$, and $\Theta(\cdot)$ being the step function. This completes the prescription of the functional.

Note that the weight functions are constructed in order to generate the Mayer bonds $f_{ij} = \exp[V_{ij}/(k_B T)] - 1$, where V_{ij} is the pair potential between particles of species i and j , upon convolution. Explicitly,

$$f_{SN}(\mathbf{r}, \mathbf{\Omega}) = -w_3^S(\mathbf{r}) * w_0^N(\mathbf{r}, \mathbf{\Omega}) - w_2^{SN}(\mathbf{r}, \mathbf{\Omega}) * w_1^N(\mathbf{r}, \mathbf{\Omega}), \quad (20)$$

$$f_{NN}(\mathbf{r}, \mathbf{\Omega}, \mathbf{\Omega}') = -2w_2^{NN}(\mathbf{r}, \mathbf{\Omega}; \mathbf{\Omega}') * w_1^N(\mathbf{r}, \mathbf{\Omega}'), \quad (21)$$

see Appendix A of Ref. 15 for the explicit calculation. By Taylor expanding Φ around $\eta=0$ one can show that the current functional is exact on the second virial level. Higher orders in η are included in an approximative way.

C. Homogeneous matrices

Considerable simplifications of the theory outlined above arise if the matrix particles are distributed uniformly in space, i.e., $\rho_S(\mathbf{r}) = \text{const}$. This still permits the study of rod orientational order, as well as inhomogeneous situations induced by an additional external influence modeled by $V_{\text{ext}}(\mathbf{r}, \mathbf{\Omega})$ in Eq. (1). The weighted densities for species i become proportional to the bulk density of species i , hence $n_v^i = \xi_v^i \rho_i$, where the proportionality constants are fundamental measures. For spheres $\xi_0^S = 1$, $\xi_2^{SN} = 4\pi R^2$, and $\xi_3^S = 4\pi R^3/3$. For rods $\xi_1^N = L/4$, $\xi_0^N = 1$, and, in an isotropic state, $n_2^{NN} = \xi_2^{NN} \rho_N$, where $\xi_2^{NN} = \pi L D$ equals the leading contribution to the surface of a rod in the limit $L/D \rightarrow \infty$. [Recall that for spherocylinders of finite aspect ratio the fundamental measures are $\xi_0 = 1$, $\xi_1 = L/4 + D/2$, $\xi_2 = \pi D(L + D)$, and $\xi_3 = \pi D^2(L/4 + D/6)$.]

The free energy density per volume for either type of matrix is then

$$\Phi_{\text{HSM}} = -n_0^N \ln(1-\eta) + \frac{(3\eta/R)n_1^N + n_1^N n_2^{NN}}{1-\eta}, \quad (22)$$

$$\Phi_{\text{IDM}} = \eta n_0^N + (3\eta/R)n_1^N + \exp(\eta)n_1^N n_2^{NN}, \quad (23)$$

where the explicit dependence of all rod weighted densities on variables is $n_v^N(\mathbf{r}, \mathbf{\Omega})$, and the sphere packing fraction η is just a constant.

D. Isotropic-nematic transition

1. Hard sphere matrix

In isotropic and homogeneous bulk states the free energy is obtained by applying the density functional to constant

density fields of spheres and rods. The resulting excess Helmholtz free energy per system volume V is given by

$$\frac{F_{\text{exc}}}{k_B T V} = -\rho_N \ln \alpha + \frac{\pi \rho_N^2 L^2 D}{4(1-\eta)}, \quad (24)$$

$$\alpha = (1-\eta) \exp\left(-\frac{3L}{2\sigma} \frac{\eta}{1-\eta}\right), \quad (25)$$

where α has the interpretation of a free volume fraction of a rod in a sea of spheres (i.e., the ratio of average volume accessible to the rods and the total volume).

In a spatially homogeneous, but orientational ordered phase (i.e., a bulk nematic) additional simplifications arise in the free energy density, Eq. (23),

$$\Phi_{\text{HSM}} = \rho_N \left[-\ln(1-\eta) + \frac{3L}{4R} \frac{\eta}{1-\eta} \right] + \frac{n_1^N(\mathbf{\Omega}) n_2^{NN}(\mathbf{\Omega})}{1-\eta}, \quad (26)$$

where ρ_N is the (bulk) rod number density. The only dependence on the orientational distribution is through the numerator of the second term on the right-hand side of Eq. (26); the denominator is a trivial constant. The specific combination of weighted densities is precisely the Onsager functional, restated in FMT terminology, see the end of Sec. III B. The effect of the denominator, however, is to *increase* the excess free energy as η grows. Note further that the first term on the right-hand side of Eq. (26) is linear in ρ_N , and hence does not affect phase equilibria. Hence we can immediately obtain the isotropic-nematic phase transition within the present theory by rescaling the known bulk (i.e., in the absence of matrix particles) solution. We find that the densities of the coexisting isotropic phase $\rho_{N,\text{iso}}$ and the nematic phase $\rho_{N,\text{nem}}$ are

$$\frac{\rho_{N,\text{iso}}}{\rho_{N,\text{iso}}^0} = \frac{\rho_{N,\text{nem}}}{\rho_{N,\text{nem}}^0} = (1-\eta), \quad (27)$$

where the coexisting densities in bulk are $(\pi/4)\rho_{N,\text{iso}}^0 L^2 D = 4.189$ in the isotropic phase and $(\pi/4)\rho_{N,\text{nem}}^0 L^2 D = 5.336$ in the nematic phase.²⁸ It might at first glance be surprising that the densities of the coexisting states in the matrix are smaller than those without matrix. This is, however, simply due to the occupied matrix volume that depletes rods. More relevant is the ratio of density of rods in the free volume left by the quenched spheres and that in bulk (without matrix). This is

$$\frac{\rho_{N,\text{iso}}}{\alpha \rho_{N,\text{iso}}^0} = \frac{\rho_{N,\text{nem}}}{\alpha \rho_{N,\text{nem}}^0} = \exp\left(\frac{3L}{2\sigma} \frac{\eta}{1-\eta}\right), \quad (28)$$

which is an *increasing* function of η , in accordance with physical expectation, as higher rod densities are required to induce the nematic order against the quenched matrix disorder. For large size ratios L/σ the effect is stronger, however, the overall analysis is, as stated above, restricted to $LD \ll \sigma^2$, hence the limit $L/\sigma \rightarrow \infty$ is not directly accessible.

2. Ideal sphere matrix

Carrying out the same analysis as above for the case of freely overlapping matrix spheres yields

$$\frac{F_{\text{exc}}}{k_B T V} = -\rho_N \ln \alpha + \frac{\pi}{4} \rho_N^2 L^2 D \exp(\eta), \quad (29)$$

$$\alpha = \exp\left[-\eta\left(1 + \frac{3L}{2\sigma}\right)\right]. \quad (30)$$

In the nematic phase

$$\Phi_{\text{IDM}} = \rho_N \eta \left(1 + \frac{3L}{4R}\right) + \exp(\eta) n_1^N(\Omega) n_2^{NN}(\Omega). \quad (31)$$

The bare coexisting densities of the isotropic and the nematic phase decrease as a function of η :

$$\frac{\rho_{N,\text{iso}}}{\rho_{N,\text{iso}}^0} = \frac{\rho_{N,\text{nem}}}{\rho_{N,\text{nem}}^0} = \exp(-\eta). \quad (32)$$

However, the actual rod density in the free volume is again increasing at coexistence,

$$\frac{\rho_{N,\text{iso}}}{\alpha \rho_{N,\text{iso}}^0} = \frac{\rho_{N,\text{nem}}}{\alpha \rho_{N,\text{nem}}^0} = \exp\left(\frac{3L}{2\sigma} \eta\right). \quad (33)$$

The increase is weaker than in the above case of the hard sphere matrix [Eq. (28)], as the present matrix induces a more open void structure due to sphere overlaps.

IV. COMPUTER SIMULATION TECHNIQUE

We have carried out Monte Carlo simulations to obtain results for the partition coefficient, defined as the ratio of densities in the matrix and in the reservoir (free of matrix spheres) in chemical equilibrium with the system ρ_N/ρ_N^r . We perform simulations of hard spherocylinders for a fixed matrix configurations and for the bulk simultaneously in two separate simulation boxes. The linear dimension of the cubic simulation boxes is about $5L$ and periodic boundary conditions are applied. Matrix configurations are taken to be equilibrated hard sphere configurations of the prescribed packing fraction η . Most of the results presented below are for a length-to-diameter ratio $L/D=20$ of the spherocylinders, while the rod-sphere size ratio is chosen to be $L/\sigma=1$. Moreover, the boxes can exchange spherocylinders in order to ensure equal chemical potential of the rods in bulk and in the matrix, while the total number of spherocylinders in the two boxes is kept constant. Typical particle numbers are ≤ 60 spheres and ≤ 12000 rods. We measure the averaged number densities of the spherocylinders in bulk and in the matrix to obtain the (averaged) partition coefficient ρ_N/ρ_N^r . To approach the Onsager limit, we have also carried out simulations for thinner rods with $L/D=80$ and 800 . Such aspect ratios severely limit the maximum obtainable reduced density $c = (\pi/4) \rho_N L^2 D$.

We also performed Monte Carlo simulations in the canonical ensemble to estimate the isotropic-nematic transition as a function of the matrix packing fraction η . We measure as a function of the reduced density of the rods c , the nematic order parameter S defined as the largest eigenvalue of the standard nematic order parameter tensor

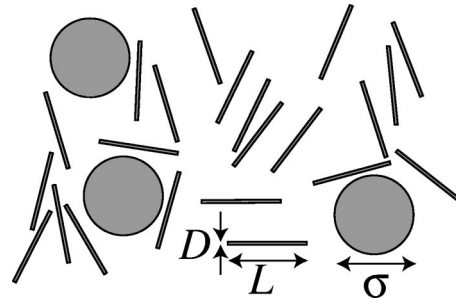


FIG. 1. Illustration of the model of hard rods of length L and diameter D immersed in a matrix of fixed hard spheres of diameter σ . The rods are equilibrated in the presence of quenched configurations of spheres. The statistical distribution of spheres is that of a pure hard sphere system.

$$Q_{\nu\tau} = \left\langle \frac{1}{N_N} \sum_{i=1}^{N_N} \left(\frac{3}{2} \Omega_\nu^{(i)} \Omega_\tau^{(i)} - \frac{\delta_{\nu\tau}}{2} \right) \right\rangle, \quad (34)$$

where $\Omega_\nu^{(i)}$ is the ν component of the unit orientation vector of particle i , N_N is the number of spherocylinders, and $\delta_{\nu\tau}$ is the Kronecker delta. At sufficiently low rod densities, S is about zero, which corresponds to the isotropic phase. We observe a jump in S upon increasing c , denoting a transition from the isotropic to nematic phase. The densities at which the jump in S occurs gives us a rough estimate of the coexisting densities of the isotropic-nematic transition. It is worth noting that the coexisting densities of the isotropic and nematic phase in bulk can be determined more accurately using Gibbs ensemble Monte Carlo simulations.²⁹ In these simulations the two coexisting phases are simulated simultaneously in two separate boxes which can exchange particles and volume to ensure equal chemical potential and equal pressure. However, Gibbs ensemble Monte Carlo simulations cannot be used to determine phase equilibria in systems at a fixed matrix packing fraction η as it is impossible to exchange volume between the two simulation boxes while keeping η fixed (see, however, Ref. 30). While histogram reweighting (see, e.g., Ref. 31) does not suffer from this problem, we expect it to be difficult to sample accurately the two phases of different symmetry with greatly differing values of the order parameter in both phases.

V. RESULTS

As a first check of the accuracy of the DFT we compare results for the partition coefficient, ρ_N/ρ_N^r , to those from MC simulation in Fig. 2. The DFT results are obtained from the (analytic) expression for the rod chemical potential obtained as $\mu_N(\rho_N, \eta) = V^{-1} \partial(F_{\text{id}} + F_{\text{exc}}) / \partial \rho_N$ and inserted into the condition for chemical equilibrium (with respect to exchange of rods) of the reservoir and the system $\mu_N(\rho_N, \eta) = \mu_N(\rho_N^r, 0)$, which is solved numerically. For fixed matrix sphere packing fraction η , there is a slow increase of ρ_N/ρ_N^r as a function of the reservoir density ρ_N^r . Simulation results are shown for reduced reservoir densities $c^r = (\pi/4) \rho_N^r L^2 D \leq 2.5$, about halfway of the density of the isotropic phase at isotropic-nematic coexistence in bulk in the case of the Onsager limit and close to the result for $L/D=20$ (see Ref. 32). In this regime the acceptance prob-

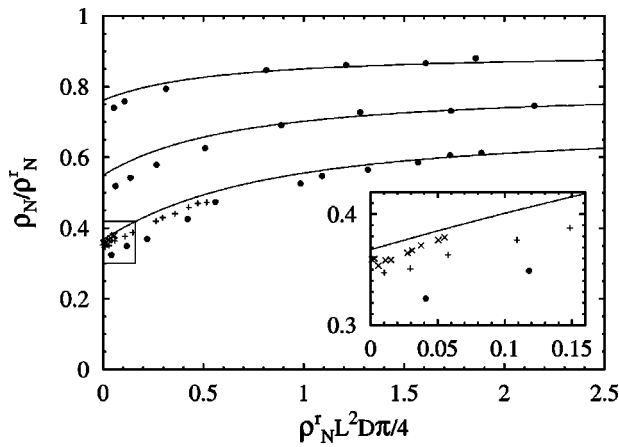


FIG. 2. Partition coefficient ρ_N/ρ_N^r , where ρ_N is the density of rods in the hard sphere matrix and ρ_N^r is the density of rods in a reservoir, as a function $\rho_N^r L^2 D \pi/4$ for packing fractions of the hard sphere matrix $\eta=0.1,0.2,0.3$ (from top to bottom) and size ratio $L/\sigma=1$. Results from DFT (lines) and from simulations (symbols) are shown. Simulation results are shown for rod aspect ratios of $L/D=20$ (dots), 80 (pluses), 800 (crosses); theoretical results correspond to the limit $L/D \rightarrow \infty$. The inset shows the area inside the rectangle marked in the main plot on an expanded scale; the simulation results approach the theoretical curve for increasing L/D .

ability of particle swaps between system and reservoir in the simulation is sufficiently large in order to obtain reliable data. Most of our simulations are carried out for an aspect ratio of $L/D=20$. The DFT results (derived in the Onsager limit, $L/D \rightarrow \infty$) overestimate slightly the MC data for small ρ_N^r , but these deviations decrease for increasing ρ_N^r . In order to assess the influence of finite rod thicknesses we have also carried out simulation runs for larger aspect ratios of $L/D=80$ and 800. Due to the scaling of c and c^r with $L^2 D$ these large values significantly limit the accessible values of c with reasonable particle numbers. It is, however, evident that for small ρ_N^r the theoretical curve is indeed approached for increasing L/D . We hence conclude that the DFT gives good account of the thermodynamic properties of isotropic states of rods in a quenched sphere matrix.

As derived in Sec. III D the DFT predicts the first-order isotropic-nematic transition to remain stable for $\eta > 0$. In Fig. 3 the results for the coexistence densities are displayed as a function of sphere packing fraction η . An almost linear decrease with η is found, which might seem at first glance surprising. The reason is that ρ_N is the average density in the system, hence both the volume of the void space between spheres and the forbidden (for rods) volume contribute. The latter clearly increases with η leading to the observed decrease in transition densities. We also display in Fig. 3 estimates of the transition densities from simulations. Those values are obtained from analysis of the nematic order parameter (as described below) obtained for $L/D=20$. For this size ratio the scaled coexistence densities are considerably smaller than in the Onsager case for $\eta=0$. The decrease of the coexistence densities upon increasing η is very similar to that predicted by the theory.

Next we investigate the behavior of the rod density in the void space of the matrix, i.e., the number of rods divided by their accessible volume rather than the total system vol-

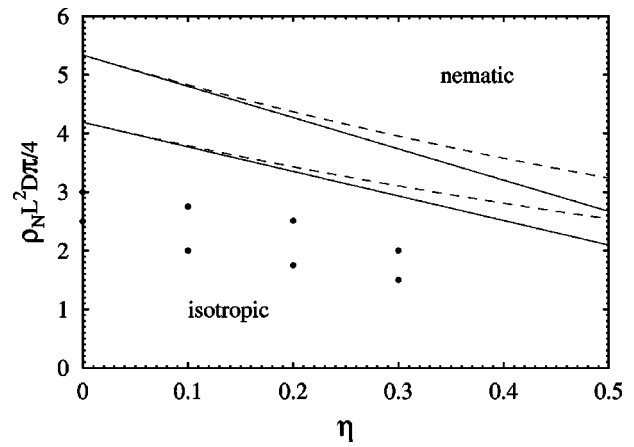


FIG. 3. Phase diagram of hard rods immersed in a matrix of quenched hard spheres displayed as a function of matrix packing fraction η and scaled rod density $\rho_N L^2 D \pi/4$. Shown are DFT results for the binodal of the isotropic-nematic transition of Onsager rods (i.e., $L/D \rightarrow \infty$) inside the hard sphere matrix (solid lines) and inside the ideal matrix (dashed lines). Coexistence is along vertical tie lines (not shown). In this representation the phase diagram is predicted to be independent of the rod-sphere size ratio L/σ . Simulation results are shown for coexistence densities (obtained from analysis of the nematic order parameter) inside the HS matrix for $L/D=20$ (symbols).

ume. This density is obtained as $\alpha^{-1} \rho_N L^2 D \pi/4$, where α is the free volume fraction accessible to the rods as given in Eq. (25) for hard sphere matrices and in Eq. (30) for ideal matrices. The results, as displayed in Fig. 4, indicate a strong increase with η . Hence larger *effective* rod densities are needed to overcome the quenched disorder and drive the system into a nematic state.

We next turn to the simulation results of the nematic order parameter, from which the coexistence densities in Fig. 3 were obtained. In Fig. 5 we plot S as a function of c for different values of η . The results for the bulk, $\eta=0$, serve as a reference case. In the isotropic state $S \approx 0.05$, which is >0 only due to the finite system size. At sufficiently high c , we observe a jump in S from which we can estimate the coexistence densities as $c_{\text{iso}}=2.5$ and $c_{\text{nem}}=3.0$, in fair accordance with data from the literature. For $L/D=20$ the coex-

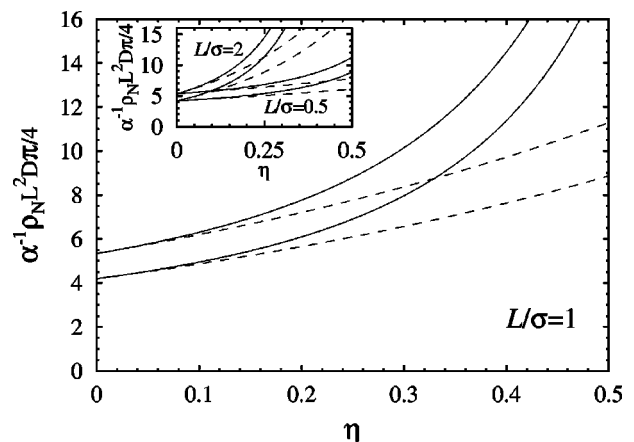


FIG. 4. Same as Fig. 3, but as a function of matrix packing fraction η and density of rods in the void space, i.e., $\alpha^{-1} \rho_N L^2 D \pi/4$, where α is the free volume fraction accessible to the rods. The inset shows the results for size ratios $L/\sigma=0.5$ and 2 (as indicated).

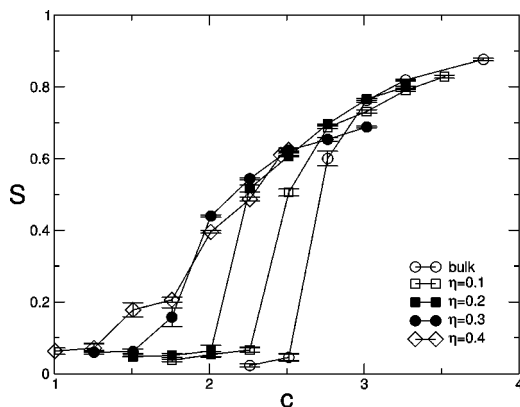


FIG. 5. Simulation results for the nematic order parameter S as a function of the scaled rod density $c = \rho_N L^2 D \pi / 4$ for different matrix sphere packing fraction $\eta = 0$ (bulk), 0.1, 0.2, 0.3.

isting phases in bulk (i.e., $\eta = 0$) have densities of $c = 2.645$ (isotropic phase) and 3.337 (nematic phase) as obtained from Gibbs ensemble simulations and $c = 2.698$ (isotropic phase) and $c = 3.315$ (nematic phase) as obtained from Kofke integration.³² Remarkably, for increasing values of sphere packing fraction, $\eta = 0.1, 0.2$, the qualitative shape of the order parameter S as a function of density c remains the same as for $\eta = 0$, hence there can still be a transition region identified. However, a marked shift to lower values of c occurs. Also the order parameter in the nematic phase attains smaller values as compared to that at the bulk transition. For the very large matrix packing fraction $\eta = 0.4$ no reliable indication of a phase transition can be determined.

We have checked that these results do not sensitively depend on the matrix configuration. In Fig. 6 results for S for the same matrix packing fraction $\eta = 0.3$, but different (random) configurations of the matrix are shown. The systematic deviations between results for different matrix configurations are comparable to the statistical error (of the annealed average).

As further illustrations of the remarkable stability of the nematic phase we display snapshots from the MC simulation in the isotropic and in the nematic phase. In Fig. 7 configurations for $c = 2.0$ and $c = 2.75$ are shown for $\eta = 0.1$, clearly

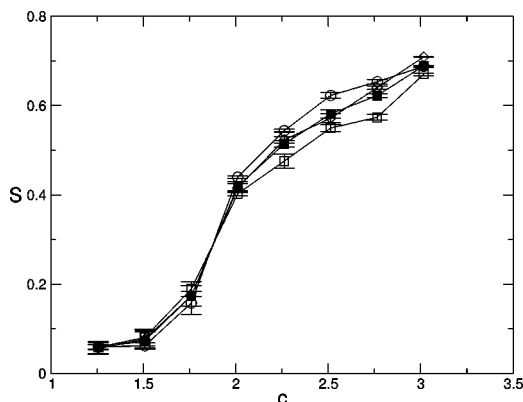


FIG. 6. Simulation results for the nematic order parameter S as a function of the scaled rod density c for fixed matrix sphere packing fraction $\eta = 0.3$ and three different realizations of the quenched hard sphere matrix.

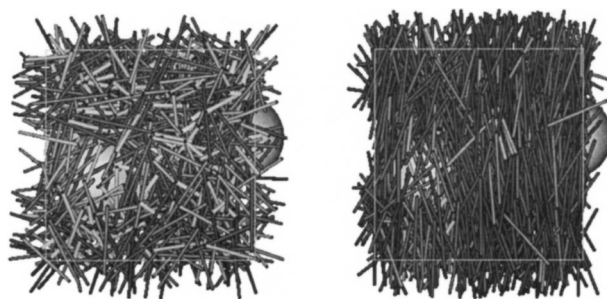


FIG. 7. Snapshots from MC simulation at statepoints close to isotropic-nematic coexistence of hard rods of aspect ratio $L/D = 20$ immersed in a matrix of quenched hard spheres of packing fraction $\eta = 0.1$. The reduced density of rods is $c = 2.0$ (isotropic phase, left) and $c = 2.75$ (nematic phase, right). Rods are colored according to their orientation.

resembling closely a bulk situation without matrix particles. In our simulations the overall director orientation is determined by the initial condition. Although there should be an optimal global director orientation for each different geometry of the void structure, in practice the system hardly changes its initial director during the course of the simulation. For $\eta = 0.2$, displayed in Fig. 8, we observe different competing local directors, especially close to the parts of the sphere surfaces normal to the global nematic director. The disturbance of the nematic phase is even more pronounced for $\eta = 0.3$, as displayed in Fig. 9.

While the theory predicts artificially the existence of an isotropic-nematic transition for all $\eta < 1$, the simulation results suggest that the transition disappears for matrix packing fractions larger than about $\eta = 0.3$. We did not focus on the precise nature of this disappearance and the question of whether it is accompanied by a critical point.

VI. CONCLUSIONS

In conclusion, we have considered the nematic-isotropic phase transition of rodlike particles immersed in a model porous medium represented by quenched hard spheres. We have used hard spherocylinders as a truly microscopic model for the steric interactions between elongated molecules or colloidal rods, and have employed DFT and Monte Carlo (MC) simulation to investigate the isotropic-nematic phase transition. As the theory is mean field in character, true long-range order and quasi-long-range order in the nematic phase cannot be distinguished. Also nematic glass phases are out of the scope of the current equilibrium approach. Within these

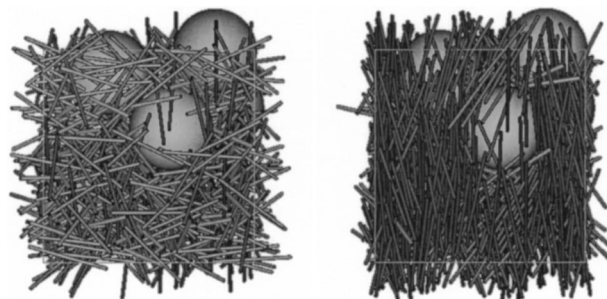


FIG. 8. Same as Fig. 7, but for $\eta = 0.2$, $c = 1.75$ (left) and $c = 2.51$ (right).

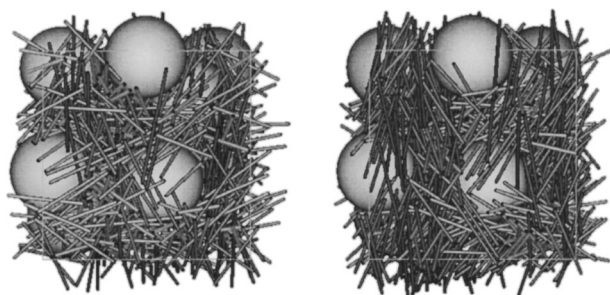


FIG. 9. Same as Fig. 8, but for $\eta=0.3$, $c=1.5$ (left) and $c=2.0$ (right).

limitations we find that the density of rods in the void structure of the matrix necessary to induce nematic order increases strongly with matrix packing fraction (exponential in the case of the ideal matrix and stronger than exponential for the hard sphere matrix). These findings are supported by MC simulation results, that clearly demonstrate the existence of nematic ordering, and the possibility of a first-order isotropic-nematic transition. As an outlook on possible future work, we mention the behavior of fluids of rodlike particles near curved surfaces³³ in the nematic phase. Furthermore it would be fascinating to experimentally test our predictions, i.e., using optical tweezers^{34–36} to fix colloidal spheres as a model porous matrix and investigate the behavior of, e.g., suspended colloidal silica rods,³⁷ favorably in real space using confocal microscopy. Including the influence of (length) polydispersity is an interesting issue that will further enrich the phase behavior (see, e.g., Refs. 38–41 for recent work of the matrix-free hard rod system).

ACKNOWLEDGMENTS

The authors thank René van Roij and Ubbo Felderhof for useful discussions. This work is part of the research program of the Stichting voor Fundamenteel Onderzoek der Materie (FOM), that is financially supported by the Nederlandse Organisatie voor Wetenschappelijk Onderzoek (NWO). Support by the DFG SFB TR6 “Physics of colloidal dispersions in external fields” is acknowledged.

¹Y. Imry and S. Ma, Phys. Rev. Lett. **35**, 1399 (1975).

²T. Bellini, M. Buscaglia, C. Chiccoli, F. Mantegazza, P. Pasini, and C. Zannoni, Phys. Rev. Lett. **85**, 1008 (2000).

³T. Bellini, M. Buscaglia, C. Chiccoli, F. Mantegazza, P. Pasini, and C. Zannoni, Phys. Rev. Lett. **88**, 245506 (2002).

⁴D. E. Feldman, Phys. Rev. Lett. **84**, 4886 (2000).

⁵J. Chakrabarti, Phys. Rev. Lett. **81**, 385 (1998).

⁶B. U. Felderhof, Physica A **323**, 88 (2003).

⁷H. Stark, J. Fukuda, and H. Yokoyama, Phys. Rev. Lett. **92**, 205502 (2004).

⁸L. Onsager, Ann. N.Y. Acad. Sci. **51**, 627 (1949).

⁹R. Evans, in *Fundamentals of Inhomogeneous Fluids*, edited by D. Henderson (Dekker, New York, 1992), Chap. 3, p. 85.

¹⁰Y. Rosenfeld, Phys. Rev. Lett. **63**, 980 (1989).

¹¹Y. Rosenfeld, Phys. Rev. E **50**, R3318 (1994).

¹²Y. Rosenfeld, Mol. Phys. **86**, 637 (1995).

¹³G. Cinacchi and F. Schmid, J. Phys.: Condens. Matter **14**, 12223 (2002).

¹⁴M. Schmidt, Phys. Rev. E **63**, 050201(R) (2001).

¹⁵J. M. Brader, A. Esztermann, and M. Schmidt, Phys. Rev. E **66**, 031401 (2002).

¹⁶A. Esztermann and M. Schmidt, Phys. Rev. E (to be published).

¹⁷R. Roth, R. van Roij, D. Andrienko, K. R. Mecke, and S. Dietrich, Phys. Rev. Lett. **89**, 088301 (2002).

¹⁸P. G. Bolhuis, J. M. Brader, and M. Schmidt, J. Phys.: Condens. Matter **48**, S3421 (2003).

¹⁹R. Roth, J. M. Brader, and M. Schmidt, Europhys. Lett. **63**, 549 (2003).

²⁰M. Schmidt, Phys. Rev. E **66**, 041108 (2002).

²¹H. Reich and M. Schmidt, J. Stat. Phys. **116**, 1683 (2004).

²²M. Schmidt, E. Schöll-Paschinger, J. Köfinger, and G. Kahl, J. Phys.: Condens. Matter **14**, 12099 (2002).

²³P. P. F. Wessels, M. Schmidt, and H. Löwen, Phys. Rev. E **68**, 061404 (2003).

²⁴M. Schmidt, Phys. Rev. E **68**, 021106 (2003).

²⁵M. Schmidt, L. Lafuente, and J. A. Cuesta, J. Phys.: Condens. Matter **15**, 4695 (2003).

²⁶M. Schmidt and J. M. Brader, J. Chem. Phys. **119**, 3495 (2003).

²⁷P. M. Johnson and C. M. van Kats (private communication).

²⁸G. J. Vroege and H. N. W. Lekkerkerker, Rep. Prog. Phys. **55**, 1241 (1992).

²⁹D. Frenkel and B. Smit, *Understanding Molecular Simulations*, 2nd ed. (Academic, San Diego, 2002).

³⁰See, however, J. K. Brennan and W. Dong, J. Chem. Phys. **116**, 8948 (2002).

³¹M. Alvarez, D. Levesque, and J. J. Weis, Phys. Rev. E **60**, 5495 (1999).

³²P. G. Bolhuis and D. Frenkel, J. Chem. Phys. **106**, 666 (1997).

³³B. Groh and S. Dietrich, Phys. Rev. E **59**, 4216 (1999).

³⁴J. P. Hoogenboom, D. L. J. Vossen, C. Faivre-Moskalenko, M. Dogterom, and A. van Blaaderen, Appl. Phys. Lett. **80**, 4828 (2002).

³⁵D. G. Grier, Nature (London) **424**, 810 (2003).

³⁶D. L. J. Vossen, J. P. Hoogenboom, K. Overgaag, and A. van Blaaderen, in *Nanopatterning—From Ultralarge-Scale Integration to Biotechnology*, edited by L. Merhari *et al.* (Materials Research Society, Boston, 2002), Vol. 705, p. Y6.8.1.

³⁷C. M. van Kats, P. M. Johnson, J. E. A. M. van den Meerakker, and A. van Blaaderen, Langmuir (to be published).

³⁸H. H. Wensink and G. J. Vroege, J. Chem. Phys. **119**, 6868 (2003).

³⁹A. Speranza and P. Sollich, J. Chem. Phys. **117**, 5421 (2002).

⁴⁰A. Speranza and P. Sollich, J. Chem. Phys. **118**, 5213 (2003).

⁴¹A. Speranza and P. Sollich, Phys. Rev. E **67**, 061702 (2003).